Assessing the Effectiveness of an Urban CO2 Monitoring Network over the Paris Region through the COVID-19 Lockdown Natural Experiment

Jinghui Lian, Thomas Lauvaux, Hervé Utard, Francois-Marie Breon, Grégoire Broquet, Michel Ramonet, Olivier Laurent, Ivonne Albarus, Karina Cucchi, Philippe Ciais

Assessing the effectiveness of an urban CO_2 monitoring network over the Paris region through the COVID-19 lockdown natural experiment

Jinghui Lian[1,2,], Thomas Lauvaux[2], Hervé Utard[1], François-Marie Bréon[2], Grégoire Broquet[2], Michel Ramonet[2], Olivier Laurent[2], Ivonne Albarus[1,2], Karina Cucchi[1] and Philippe Ciais[2,3]*

[1] Origins.S.A.S, Suez Group, Tour CB21, 16 Place de l'Iris, 92040 Paris La Défense Cedex, France

[2] Laboratoire des Sciences du Climat et de l'Environnement (LSCE), IPSL, CEA-CNRS-UVSQ, Université Paris-Saclay, 91191 Gif sur Yvette Cedex, France

[3] Climate and Atmosphere Research Center (CARE-C), The Cyprus Institute, 20 Konstantinou Kavafi Street, 2121, Nicosia, Cyprus

KEYWORDS

CO_2 emissions, city, atmospheric inversion, COVID-19 lockdown

ABSTRACT

The Paris metropolitan area, the largest urban region in the European Union, has experienced two national COVID-19 confinements in 2020 with different levels of restrictions on mobility and economic activity, which caused reductions in CO_2 emissions. To quantify the timing and

magnitude of daily emission reductions during the two lockdowns, we used continuous atmospheric CO_2 monitoring, a new high-resolution near-real-time emission inventory and an atmospheric Bayesian inverse model. The atmospheric inversion estimated the changes in fossil fuel CO_2 emissions over the Greater Paris region during the two lockdowns, in comparison with the same periods in 2018 and 2019. It shows decreases by 42~53% during the first lockdown with stringent measures, and by only 20% during the second lockdown when traffic reduction was weaker. Both lockdown emission reductions are mainly due to decreases in traffic. These results are consistent with independent estimates based on activity data made by the city environmental agency. We also show that unusual persistent anticyclonic weather patterns with north-easterly winds that prevailed at the start of the first lockdown period contributed a substantial drop in measured CO_2 concentration enhancements over Paris, superimposed on the reduction of urban CO_2 emissions. We conclude that atmospheric CO_2 monitoring makes it possible to identify significant emission changes (>20%) at subannual time scales over an urban region.

SYNOPSIS

This study quantifies the impact of COVID-19 on CO_2 emissions over Paris via an inverse modeling technique using in situ atmospheric CO_2 observations.

1 Introduction

The world economy has been strongly impacted by the COVID-19 pandemic with many countries enforcing a wide range of measures to limit the spread of the virus. One side effect has been a strong reduction in fossil fuel use, which led to a reduction in global carbon emissions in the first half of 2020 as compared to the same period in 2019[1,2]. Although the emissions

recovered later in the year, 2020 emissions were reported at several percent less than those of 2019, i.e. 4% from Carbon Monitor (https://carbonmonitor.org/), 6.4% from Tollefson[3], and 7% from Le Quéré et al.[4].

At the city scale, the reduction of human and economic activities during the lockdown periods led to measurable decreases in urban anthropogenic CO_2 emissions. The COVID-19 lockdowns provide a testbed to assess the effectiveness of various methods that estimate city-scale CO_2 emissions. CO_2 gridded emission maps at fine space and time scales are more informative than city-level inventories. However, these estimates are prone to large uncertainties[5]. To constrain spatial and temporal bottom-up emission estimates, independent information is needed, which motivates the use of atmospheric measurements. Ground-based in situ continuous urban CO_2 monitoring stations are usually equipped with high-precision cavity ring-down spectroscopy (CRDS) CO_2 analyzers. Other complementary CO_2 observing systems include low-cost but lower accuracy sensors[6], localized eddy covariance flux towers[7], carbon isotope measurements[8], periodic automobile and aircraft campaigns[9], as well as satellite and remote sensing[10]. Atmospheric measurements can be collected in near-real-time and assimilated with models to constrain emissions with low latency. This is an advantage insofar because most city emission inventories have a lag of at least 1 year. The statistical approach that combines atmospheric measurements with emission inventories and high-resolution transport modeling is called urban atmospheric inversion. Over the last few years, urban inversions mainly based on Bayesian methods, combined with either Lagrangian-based or Eulerian-based atmospheric transport models have been applied to quantify CO_2 emissions on monthly time scales over several metropolitan areas, e.g., Paris, Boston, and Indianapolis[11,12,13]. However, few inversions have demonstrated the ability to detect and quantify short-term urban emission changes arising from a

63 sudden change in human activities like the COVID-19 pandemic[14]. Two recent studies have
64 quantified the reductions of emissions in the San Francisco Bay area, Los Angeles and
65 Washington DC/Baltimore metropolitan areas in the US[6,15]. These studies have used an inverse
66 method based on the Lagrangian approach. In addition, few inversions have separated emissions
67 from different districts or administrative units within a megacity, mostly because of scarce
68 atmospheric measurements.

69 In France, national authorities implemented two nationwide lockdown periods in 2020: March
70 17th to May 11th (55 days) and October 30th to December 15th (46 days). These two periods were
71 associated with reductions of mobility measures, although with marked differences, with the
72 spring confinement being much stricter than the autumn one. They provide a unique opportunity
73 to evaluate how a Eulerian-based atmospheric inversion system can quantify subannual changes
74 in urban CO_2 emissions from city centers to suburban areas in a timely manner.

75 This study analyzes CO_2 emission changes with Bayesian atmospheric inversions assimilating
76 CO_2 observations from six high-precision in situ stations located in and around the Paris
77 metropolitan area with a high-resolution WRF-Chem transport model and a newly developed
78 near-real-time emission inventory. These inversions are based on an updated version of the
79 Parisian inversion system developed by Bréon et al.[16] and Staufer et al.[11], using a well-calibrated
80 version of WRF-Chem intensely evaluated against meteorological and CO_2 measurements by
81 Lian et al.[17,18,19]. Meanwhile, compared to previous inversion studies over Paris, our observation
82 network grew with two newly built urban stations and four suburban stations operated since
83 2014. Only three suburban sites, operational during the period 2010-2011, were used by Staufer
84 et al.[11].

In the following, section 2 describes the fossil fuel CO_2 emission inventory, the CO_2 monitoring network, and the city-scale atmospheric inversion system deployed for Paris. Section 3 analyzes in detail the measured CO_2 concentrations and the inversion results. A discussion is given in section 4.

2 Methodology

2.1 Fossil fuel CO_2 emission inventory

This study uses a novel near-real-time data set of fossil fuel CO_2 emissions for the Paris region developed by Origins.earth (https://www.origins.earth). The Origins bottom-up inventory provides the Scope 1 hourly gridded CO_2 emissions over Paris from 2018 until the present time for six activity sectors, namely transportation, residential, tertiary, industry (including cement), energy, and waste. CO_2 emissions are available at the hourly time scale and at 1 km × 1 km spatial resolution (SI Appendix, Text S1).

The spatial distribution of the total fossil fuel CO_2 emissions from March 17th to May 10th for the years 2018, 2019 and 2020 shows that the emissions are highly concentrated over the city of Paris and its vicinity, mainly due to the high population density, various commercial activities and a high volume of traffic (Figure S1). With the implementation of lockdown measures in 2020, a decrease in CO_2 emissions is observed over the center of Paris and the location of highways when compared with the previous 2 years. Figure 1 shows the daily fossil fuel CO_2 emissions for 12 calendar months of the year 2020 with comparison to 2018 and 2019 over the entire domain shown in Figure S1. We group the Origins emissions into three main sectors: i) traffic which includes both on-road and nonroad transport, ii) building which includes residential and commercial activities, iii) all other emissions from the remaining sources including industry,

energy and waste. The emission budgets of the building sector are 3.43, 3.48 and 2.90 $MtCO_2$, representing 39.9%, 41.6% and 47.0% of total emissions from March to May for 2018, 2019 and 2020 respectively (Figure S2). The traffic sector emissions are of 3.30 $MtCO_2$ (38.4% of the total emissions from March to May), 2.88 $MtCO_2$ (34.5%) and 1.54 $MtCO_2$ (25.0%) from 2018 to 2020.

The lockdown measures caused a clear decrease in the total CO_2 emissions according to the Origins inventory, as well as in the diurnal and weekly variations (Figures 1 and S3). The most pronounced decline is for the traffic sector as a consequence of the mobility restrictions. A large and sudden decrease in traffic emissions was observed at the beginning of the first lockdown period, followed by a progressive increase over time. The traffic estimates remained below typical levels after the end of the first confinement until mid-June. Starting in July, the traffic emissions recovered to prepandemic levels and were at a comparable level to that of the previous years. The traffic emissions in summer showed a small reduction linked to the summer vacation period in July and August. The second lockdown period also led to a drop in CO_2 emissions, but less pronounced than the first one. Less stringent measures were adopted such as keeping schools open and more tolerance to commute to work when needed[20]. The 2019-2020 emission changes in other sectors are of a smaller magnitude than those of the traffic. Figure 1 shows that CO_2 emissions from the building and industry sectors in April and May 2020 were lower than those of 2019, which could be interpreted as a consequence of the lockdown. However, as the building emissions are very sensitive to the temperature, one must analyze the interannual temperature anomalies before reaching a causal relationship. Indeed, according to the Météo-France climate bulletin[21], April and May 2020 were 2.7°C and 2.2°C warmer than 2019, respectively, so that lower emissions are expected, without a COVID-19 effect. Further analyses[22] clearly show that,

after the correction for temperature anomalies, the daily gas consumption within the city of Paris was still lower in 2020 than it was in 2019.

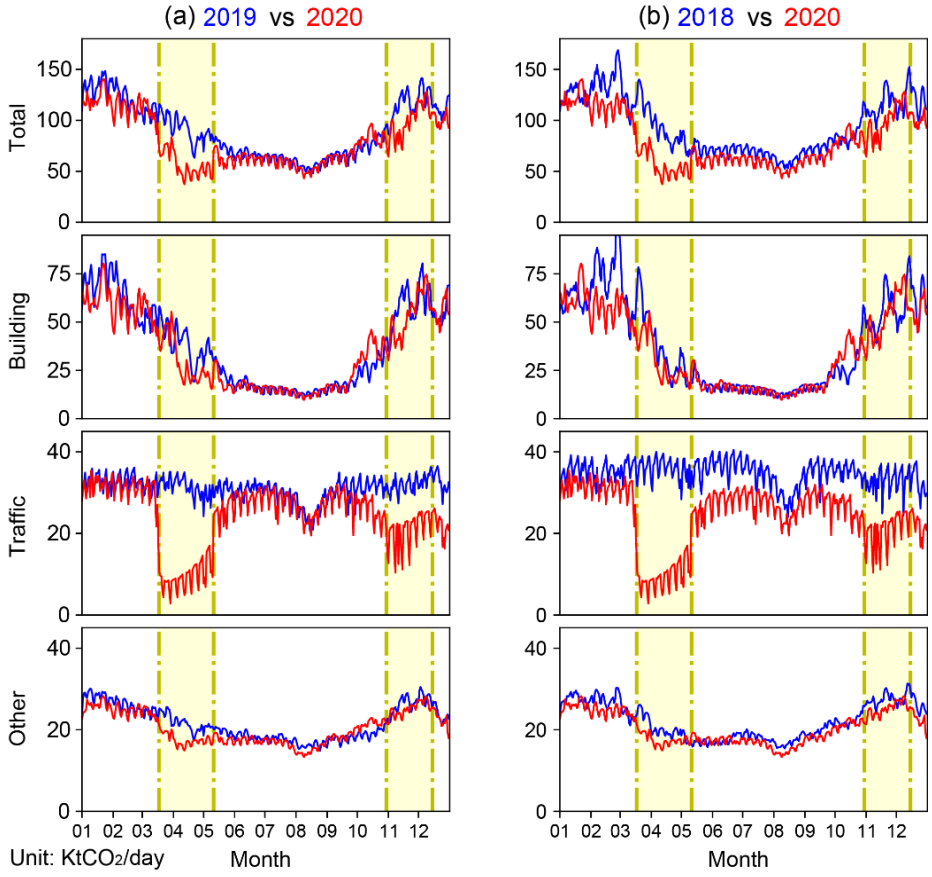

Figure 1. Comparison of the daily fossil fuel CO_2 emissions for different sectors, namely total, traffic, building (residential and commercial), other (industry, energy and waste) for 12 calendar months of the year (a) 2019 and 2020, (b) 2018 and 2020. The yellow shaded areas indicate the lockdown periods.

2.2 CO_2 monitoring network and meteorological measurements

Hourly CO_2 measurements collected at six sites, including two urban and four suburban stations, were used in this study. The locations of the stations are shown in Figure 2. Two stations (JUS and CDS) are located within the center of Paris in a dense urban environment where the emission

density is the highest. The other four stations (AND, GNS, OVS, SAC) are located at the edges of the urban and built-up areas in mixed urban-rural environments. All of these stations are equipped with high-precision CRDS CO_2 analyzers, with an accuracy that is on the order of a fraction of a ppm with reference to the World Meteorological Organization (WMO) international mole fraction scale[23]. The air sampling inlets are installed on rooftops or on towers to extend the footprint of the measurement and reduce the potential impact of local emissions. Apart from the CO_2 measurements, the hourly wind speed and wind direction are measured at a height of 100 meters above the ground level at the SAC station. The model-observation misfits for wind are used to filter the CO_2 data to be assimilated in the inversion.

2.3 City-scale atmospheric inversion system

The CO_2 atmospheric inversion system is Bayesian with priors and all error statistics being assumed to be Gaussian (SI Appendix, Text S2). The assimilation of downwind-upwind gradients in CO_2 concentrations for city-scale inversion has been used in this study[11,16,24]. Using the concentration gradients, rather than the absolute concentrations, in the assimilation system is an effective way to decrease the uncertainties in biogenic and remote fluxes[19]. The principles of the inversion used here are similar to those of Bréon et al.[16], Staufer et al.[11] and Wu et al.[24]. However, it uses a specific partition of the emissions in the Île-de-France (IdF) region to support the focus on the emissions from the Greater Paris region. Furthermore, the system has been adapted to assimilate data from the current Parisian CO_2 monitoring network, and to use the 1 km-resolution WRF-Chem transport modeling framework developed by Lian et al.[18,19] (SI Appendix, Text S3).

The inversion is applied to optimize fossil fuel emissions and biogenic fluxes from March 1st to May 31st and from October 21st to December 23rd for 2018, 2019 and 2020 respectively, which covers the two entire lockdown periods as well as the same periods in the prior 2 years. In the following, section 2.3.1 presents the reference inversion configuration. In section 2.3.2, a set of sensitivity experiments is designed to evaluate the impact of different inversion configurations on the retrieved estimates of fossil fuel CO_2 emissions.

2.3.1 Reference inversion setup

The prior fossil fuel emissions within the IdF region, which includes Paris and its neighboring departments, covering an area of 12012 km² (Figure 2), are based on the Origins inventory. Fossil fuel CO_2 emissions outside the IdF region (but included in the modeling domain, Figure S4) originate from the ODIAC Fossil Fuel CO_2 Emissions Dataset (version name: ODIAC2020) for the year 2018, also at 1×1 km horizontal resolution[25]. The ODIAC monthly budget was also multiplied by the temporal profiles to account for the weekly and diurnal cycles of the emissions[26]. Biogenic CO_2 fluxes were simulated with the diagnostic biosphere Vegetation Photosynthesis and Respiration Model (VPRM), coupled online to the WRF atmospheric model used for transporting CO_2, thus ensuring a perfect consistency between the atmospheric physics and the variability in biogenic fluxes [27,28].

The inversion controls CO_2 emissions by different control vectors that correspond to a sector of activity over a given geographic area and for a given time window. Figure 2, together with Table S1 shows the spatial (i.e. within Paris and outside Paris) and temporal (i.e. 6-hourly windows) resolutions of the control vectors used for the fossil fuel and biogenic fluxes (SI Appendix, Text S4). Concerning the partitioning of fossil fuel emissions, we divided the WRF-Chem innermost

domain (Figure S4) into three emitting regions for which the emissions can be optimized: the Greater Paris region, the rest of the IdF region, and outside the IdF region (Figure 2b). The Origins inventory estimates that the Paris city, the Greater Paris area (excluding Paris city) and the rest of the IdF region emitted 4.33, 14.67 and 16.31 $MtCO_2$, taking up 12.3%, 41.5% and 46.2% of the total fossil fuel CO_2 emissions over the whole IdF region in 2019, respectively. Note that the sizes of these three regions are significantly different, so that the emissions per unit area of Paris city is larger than those of the other two, even though its total emissions are smaller. The inversion system rescales prior estimates over 6-hour time windows (4 unknowns per day, namely 0:00-6:00, 6:00-12:00, 12:00-18:00, 18:00-0:00 UTC) of the fossil fuel emissions over the Greater Paris region (including Paris city) that is provided by the Origins inventory. In addition, we also attempt to further separate the city of Paris (red shaded area in Figure 2b) from the Greater Paris region (results shown in the discussion section). The inversion system also optimizes prior estimates of (i) 6 h fossil fuel emission budgets for the rest of the IdF region, (ii) daily fossil fuel emission budget outside the IdF region, and (iii) daily budget of biogenic fluxes (net ecosystem exchange - NEE) over the entire model innermost domain provided by the VPRM model (Table S1).

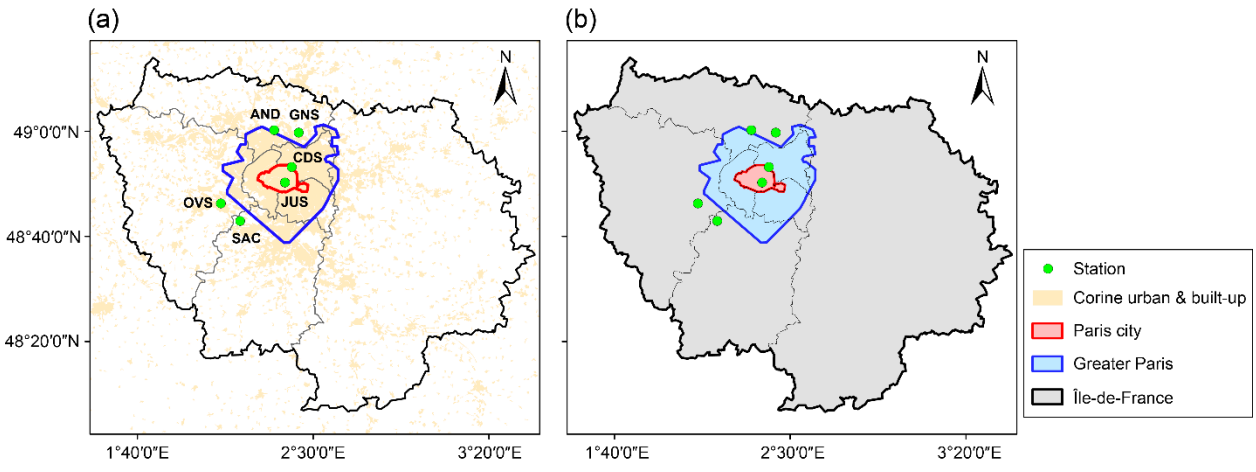

Figure 2. (a) Yellow shaded areas indicate the Corine urban and built-up land use. The city of Paris is located within the inner red line. The Greater Paris region (blue line) extends over a larger surface, following its administrative boundaries (including Paris city and the three administrative jurisdictions that are around Paris, called "Petite Couronne"). The Île-de-France region (black line) is made up of eight administrative jurisdictions, including the city of Paris, the three Petite Couronne jurisdictions and four other larger jurisdictions with a smaller population density (thin gray lines). (b) Map of the subregions whose fossil fuel emission budgets are controlled by the inversion. In the reference inversion configuration, emissions over three emitting regions are optimized independently: the Greater Paris region (red+blue shaded area), the rest of the IdF region (gray shaded area), and outside the IdF region. Data source: The Corine land cover data are available at https://land.copernicus.eu/pan-european/corine-land-cover.

The inversion system assimilates CO_2 concentration gradients between pairs of stations aligned roughly along the wind direction and respectively upwind and downwind a significant area of the city. It is assumed that the signature of remote fluxes is relatively small in such gradients that are dominated by the signature of the city emissions[11]. The method for the selection of the assimilated CO_2 downwind-upwind gradients was described in detail in Wu et al.[24] and is outlined in the SI Appendix (Text S5). The assimilated hourly afternoon CO_2 concentration gradients are given in the SI Appendix (Text S6). The inversion framework also requires prescribing the observation errors and the uncertainties in prior emissions. Assumptions regarding these error covariance matrices are similar to those of Bréon et al.[16] and Wu et al.[24], and are detailed in the SI Appendix (Text S7 and Text S8).

2.3.2 Sensitivity tests

To analyze the sensitivity of the results to the inversion configuration, 19 additional inversions were conducted (NO. 2-20 in Table S3). These tests are further classified into three groups. First, three sensitivity tests (NO. 2-4) are designed to analyze the impact of using, or not, the measurements from the two urban stations (JUS and CDS) that lie within the core of the city. Another set of inversions (NO. 5-13) allows us to analyze the sensitivity of the results to the data selection criteria of the assimilated gradients. The third set of sensitivity tests (NO. 14-20) aims at investigating the impacts of uncertainties in prior fossil fuel and biogenic fluxes, as well as their temporal correlations.

3 Results

3.1 CO_2 concentration measurements

Figure 3a shows the time series of the afternoon (12-17 UTC) averages of the observed CO_2 concentrations at JUS, an urban station located in the center of Paris, from 2018 to 2020. It shows that the observed CO_2 seasonal variability is mostly driven by the seasonality in regional-scale biogenic fluxes, whereas meteorological conditions significantly impact the short-term variations (i.e. synoptic and daily time scales). During March 2020, low-pressure systems located north of the British Isles resulted in cloudy skies over the Paris region, a common synoptic regime during winter. In mid-March, the Paris region came under the increased influence of the Azores high-pressure anticyclonic system, favoring the predominance of warm and dry weather[21]. The first lockdown period started simultaneously with a change in meteorological conditions. In addition, the aforementioned warm spring in 2020 led to an early start of the vegetation by about 1 week. Consequently, atmospheric CO_2 concentrations during the first lockdown are not only perturbed by emission reductions but are also influenced by unusual

meteorological conditions and early vegetation bloom. No anomalous weather regime nor unusual plant phenology was observed during the second lockdown.

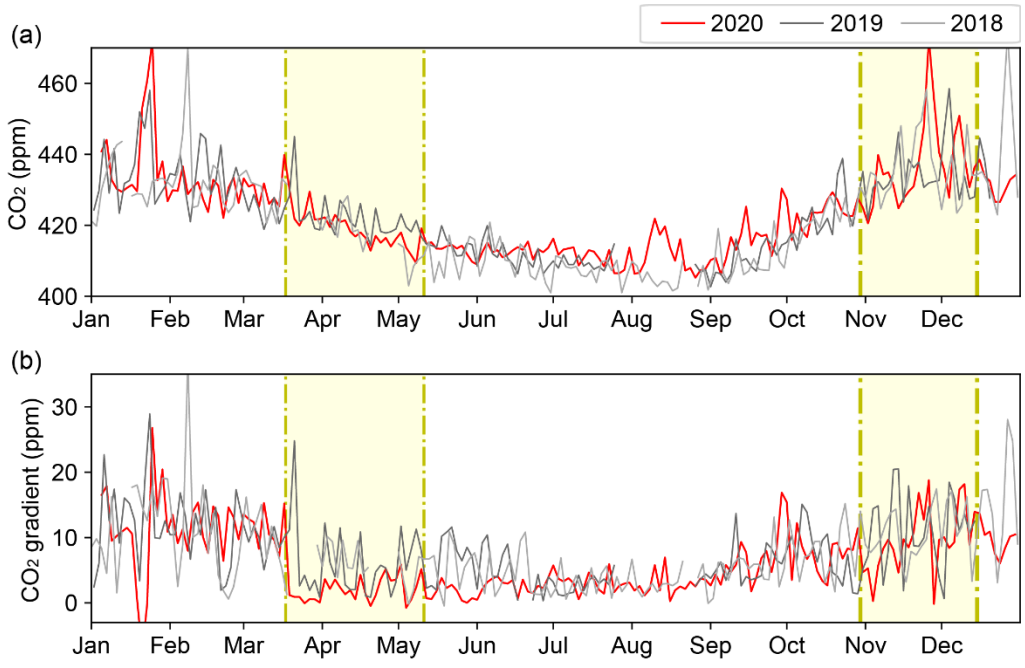

Figure 3. Two-day afternoon (12-17 UTC) mean of the observed: (a) CO_2 concentrations at the JUS station, and (b) CO_2 concentration gradients between JUS and SAC stations. The yellow shaded areas indicate the lockdown periods.

The use of CO_2 concentration gradients (downwind-upwind) reduces the impact of boundary CO_2 conditions advected into the Paris area and from remote fluxes in the model domain outside the station's network, facilitating our ability to track CO_2 signals due to fossil fuel emissions from the Paris urban area. We thus computed the differences in CO_2 concentrations between JUS and the SAC station which is located about 20 km southwest of the Paris center in a suburban area. Figure 3b shows that during the first lockdown period, a significant drop in JUS-SAC CO_2 concentration gradients is observed with a decrease of 65% when compared to the prelockdown period (SI Appendix, Text S9). However, because the synoptic weather conditions changed at the

start of the first lockdown period, analyzing the concentration gradients to determine lockdown-induced fossil fuel CO_2 signals is not possible without filtering specific conditions or using modeling tools, as noted by Ciais et al.[29]. We therefore show the JUS-SAC CO_2 concentration gradients as a function of wind direction (Figure 4). The hourly afternoon data (12-17 UTC) were classified into different classes ranging from -10 to 12 ppm in steps of 2 ppm. The figure shows the frequency and mean CO_2 difference per bin for the 16 wind direction sectors (22.5° each). For wind fields, we used wind measurements at 100 m above the ground level at the SAC station. The impact of the wind speed is presented in Figure S7, where the JUS-SAC CO_2 gradients are shown as a function of wind speed and direction.

Figure 4a shows that relatively large CO_2 concentration gradients (8~12 ppm) between JUS and SAC stations are observed during the prelockdown period with prevailing winds from the southwest. These large CO_2 gradients are most likely attributed not only to the high emissions from household heating over Paris but also to the relatively weak vertical mixing in winter. However, the dominant winds changed from southwest to northeast in mid-March 2020, simultaneously with the start of the first lockdown (Figure 4b). The CO_2 wind rose shows a small difference (0~2 ppm) between JUS and SAC in the 22.5-45° sector, which can be expected since the SAC station is downwind of Paris and thus the CO_2 variability is most likely under the influence of the emissions coming from Paris. Moreover, the decrease in CO_2 concentration gradients could also result from a deepening of the mixed layer as well as a reduced household heating demand with increasing temperature. All of these changes obscure the effect of restrictions on fossil fuel emissions during the lockdown.

To resolve this question, we compared the CO_2 wind rose during the first lockdown (Figure 4b) to those observed on average during the previous years for the same time interval (Figure 4c and

4d). In the 0-90° sector when the wind speeds are lower than 9m/s (Figure S7), the CO_2 concentration gradients between JUS and SAC are smaller in 2020 (< 2 ppm) than in 2018 and 2019 (2~4 ppm). This analysis suggests that the observed drop in the CO_2 concentration gradient in 2020 is associated with the corresponding reductions of emission sources due to the COVID-19 lockdown and cannot only be explained by the coincident shift in wind direction. Quantitative estimation of emissions and biogenic fluxes nevertheless requires an inversion with observed atmospheric transport fields during the lockdown periods.

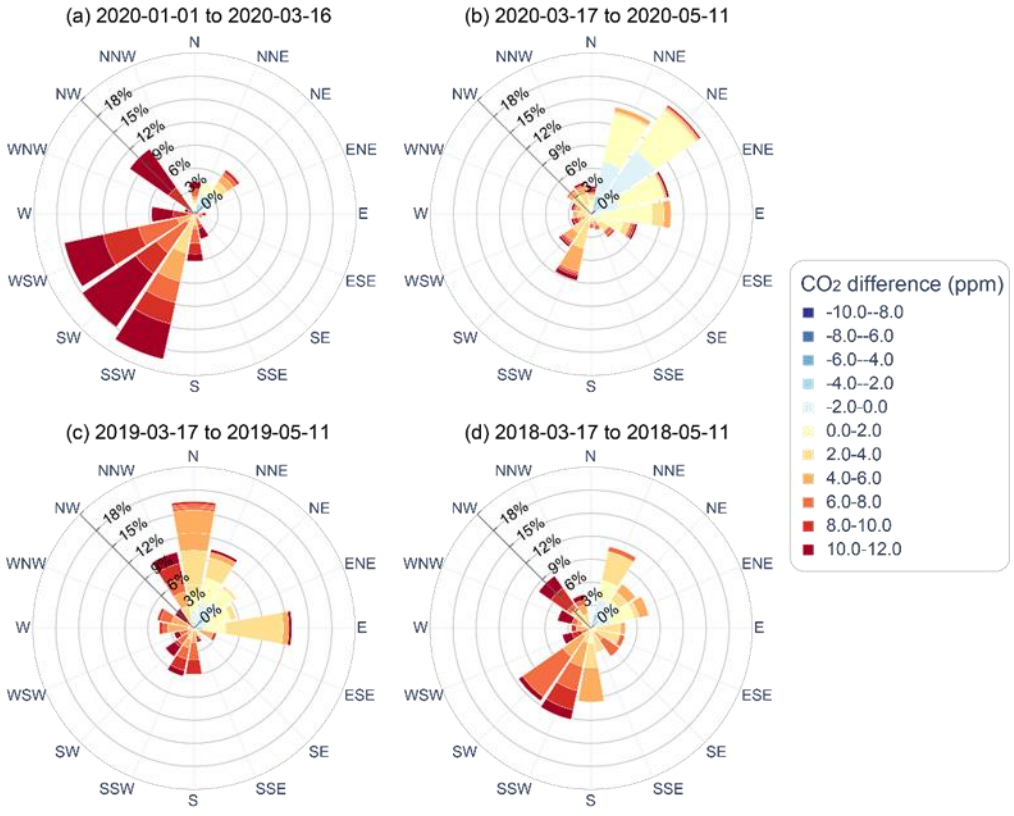

Figure 4. CO_2 concentration gradients between JUS and SAC stations as a function of wind direction over: (a) the prelockdown period from January 1st to March 16th 2020, (b)-(d) the first lockdown period from March 17th to May 11th 2020, and the same periods of the year in 2019 and 2018. The percentages on the axes indicate the frequency of CO_2 concentration differences

within each class interval when winds come from particular directions. Note that only the afternoon data (12-17 UTC) are used in the analysis.

3.2 Inversion results

We first analyze the fit between observed and simulated concentrations from prior and posterior fluxes, as an indication of the efficiency of the inversion in reducing the misfits to the observations. Figure S8 shows that the agreement between the posterior CO_2 concentration gradients as compared to the observations is substantially better than those induced by the prior fluxes (SI Appendix, Text S10).

3.2.1 Daily emission estimates

We use here the reference inversion detailed in section 2.3.1 and focus on the fossil fuel CO_2 emissions over the Greater Paris region where most of the emissions are concentrated. The inversion has little impact on the estimate of the fossil fuel fluxes over the rest of the IdF region and the biogenic fluxes (Table S4 and Figure S9), and the reasons are given in the SI Appendix (Text S11).

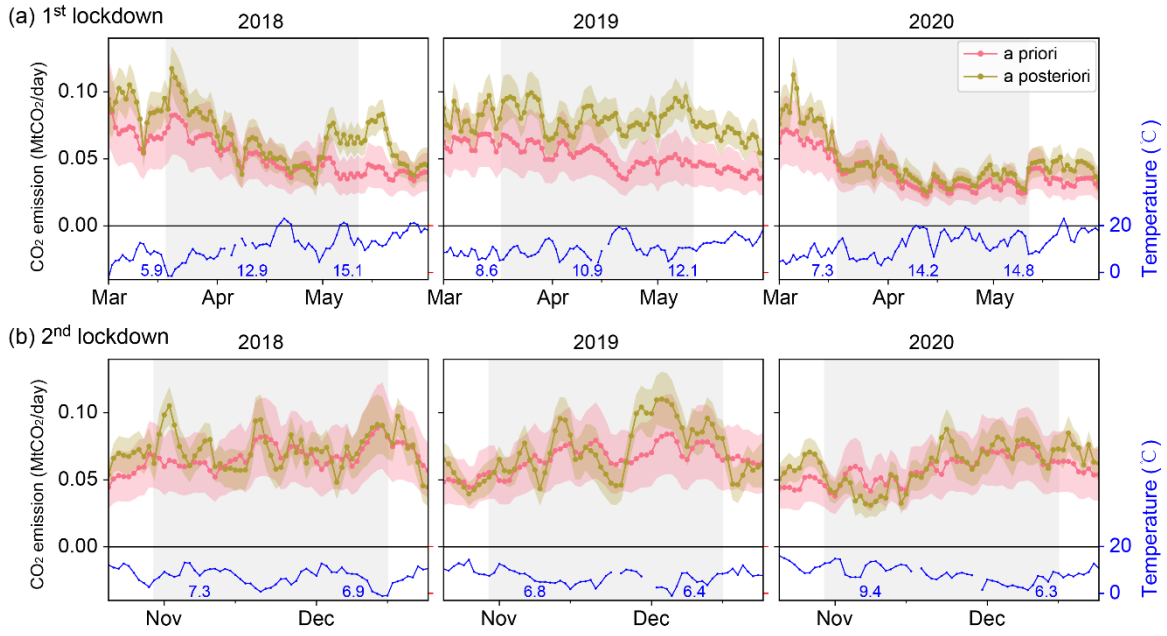

Figure 5. Daily estimates of the fossil fuel emission for the (a) March 1st - May 31st and (b) October 21st - December 23rd periods for the years 2018, 2019 and 2020 respectively over the Greater Paris region. The grey shaded areas indicate the lockdown periods. The pink line and shading show the prior flux according to the Origins inventory together with its assumed uncertainty. The yellow and shading show the posterior estimates with their uncertainty ranges. The blue lines indicate the daily mean temperature measured at 100 m above the ground level at the SAC station. Numbers in blue at the bottom denote the monthly mean temperature.

Figure 5 shows that the posterior emission estimates are generally larger than the prior ones and have larger temporal variations. Inverse emissions are mostly within the range of the prior uncertainty. The inversion leads to a reduction of the emission uncertainty by a factor of ~2. We also found a roughly inverse relationship between the daily mean temperature and daily CO_2 emissions (see the blue line in Figure 5). The highest emission increments are obtained in spring 2019, presumably related to the fact that the monthly mean temperatures in April and May 2019 were lower than those for the other 2 years, by around 2°C.

Figure 5 also illustrates modeling errors in the inversion procedure. First, the posterior estimates of the daily fluxes show deviations from the prior that might be caused by atmospheric transport model errors from day-to-day or synoptic scales. One example is the large (a factor of ~2) decrease of the a posteriori emissions from November 1st to 7th 2020. We investigated the atmospheric model behavior during this period and concluded that WRF poorly simulates stable atmospheric conditions, with an overestimate of the PBL height. We examined other periods (from May 1st to 15th 2018) when the posterior emissions are much larger than the prior, but the simulated meteorological fields (i.e. temperature, wind and PBL height) agree reasonably well with the observations and are not correlated with cold days, suggesting that some of the observed weekly changes might be due to activity changes.

Second, it appears that day-to-day variations of the inverse emissions are also driven by the amount of atmospheric data used. Indeed, because of the selection criteria, the number of assimilated gradients varies considerably from one day to another (Figures S5 and S6). When few or no concentration gradients fit the assigned criteria on a given day, the temporal variations in the inverse emissions rely on observations over neighboring days. A typical example is the period around November 25th 2019. The inverse emissions show a gradual decrease with large posterior uncertainties up to this date, followed by a very sharp increase (factor of more than 2). Further analysis shows that the measured concentration gradients are smaller than those modelled on the 25th, and larger afterward, which explains the sharp increase. There are no valid observations for the period from November 16th to 24th, so the posterior estimates start from the prior, and decrease toward the estimates controlled by the observations of the 25th, because of the prescribed 7-day error correlation length for the fossil fuel emissions.

3.2.2 CO_2 emissions budgets during the lockdown

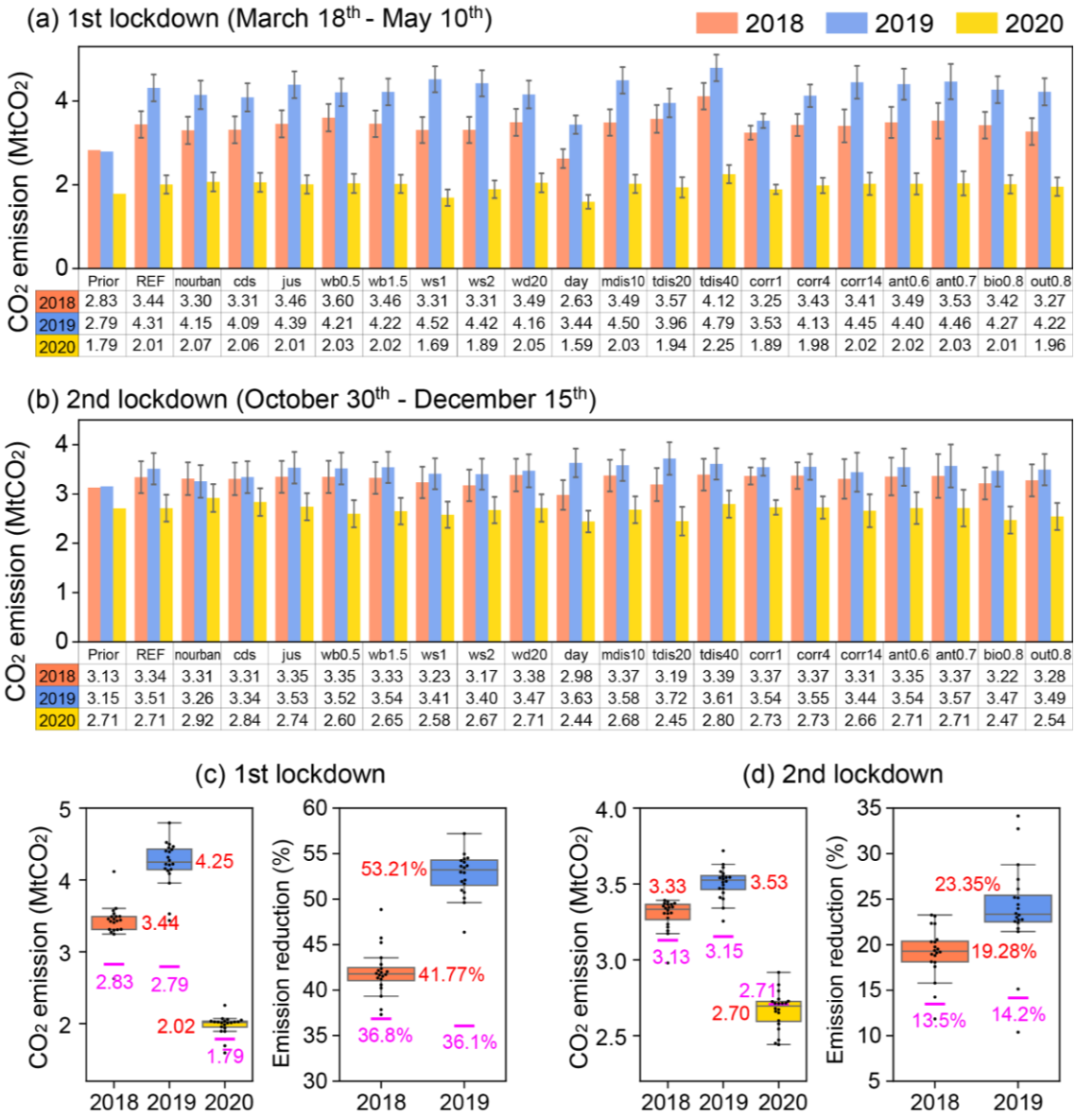

	Prior	REF	nourban	cds	jus	wb0.5	wb1.5	ws1	ws2	wd20	day	mdis10	tdis20	tdis40	corr1	corr4	corr14	ant0.6	ant0.7	bio0.8	out0.8
2018	2.83	3.44	3.30	3.31	3.46	3.60	3.46	3.31	3.31	3.49	2.63	3.49	3.57	4.12	3.25	3.43	3.41	3.49	3.53	3.42	3.27
2019	2.79	4.31	4.15	4.09	4.39	4.21	4.22	4.52	4.42	4.16	3.44	4.50	3.96	4.79	3.53	4.13	4.45	4.40	4.46	4.27	4.22
2020	1.79	2.01	2.07	2.06	2.01	2.03	2.02	1.69	1.89	2.05	1.59	2.03	1.94	2.25	1.89	1.98	2.02	2.02	2.03	2.01	1.96

	Prior	REF	nourban	cds	jus	wb0.5	wb1.5	ws1	ws2	wd20	day	mdis10	tdis20	tdis40	corr1	corr4	corr14	ant0.6	ant0.7	bio0.8	out0.8
2018	3.13	3.34	3.31	3.31	3.35	3.35	3.33	3.23	3.17	3.38	2.98	3.37	3.19	3.39	3.37	3.37	3.31	3.35	3.37	3.22	3.28
2019	3.15	3.51	3.26	3.34	3.53	3.52	3.54	3.41	3.40	3.47	3.63	3.58	3.72	3.61	3.54	3.55	3.44	3.54	3.57	3.47	3.49
2020	2.71	2.71	2.92	2.84	2.74	2.60	2.65	2.58	2.67	2.71	2.44	2.68	2.45	2.80	2.73	2.73	2.66	2.71	2.71	2.47	2.54

Figure 6. Sensitivity results for the estimates of the total fossil fuel CO_2 emission budgets during the (a) (c) first and (b) (d) second lockdown periods over the Greater Paris region (including Paris) for the years 2018, 2019 and 2020. Panels (c) and (d) present the distribution of the prior and posterior CO_2 estimates, both for the absolute emission budgets and for the relative emission reduction ratio. The midpoint, the box and the whiskers represent the 0.5 quantile, 0.25/0.75 quantiles, and 0.1/0.9 quantiles respectively. The medium values of the posterior

354 estimates among the sensitivity tests are shown in red. The prior estimates from the Origins
355 inventory are shown in magenta.

356 We then focus on the total fossil fuel CO_2 emission budgets during the first (March 18th - May
357 10th) and second (October 30th - December 15th) lockdown periods, in comparison to the same
358 period in 2018 and 2019 over the Greater Paris region. To get an indication of the robustness of
359 the inversion results, we also look at the total emission estimates obtained with the reference
360 configuration together with the sensitivity tests of the inversion configuration. In Figures 6a and
361 6b, the first column on the left (Prior) shows the prior emissions from the Origins inventory. The
362 second one (REF) shows the posterior estimates derived from the reference inversion. The other
363 columns show the posterior values based on different sensitivity tests described in Table S3, each
364 corresponding to a different set of assumptions.

365 Overall, the results for the emissions over the two lockdown periods show limited sensitivity to
366 the inversion setup. Most of the configurations tend to increase the fossil fuel CO_2 emissions
367 with respect to the prior estimates, which gives us a certain degree of confidence that our prior
368 emissions were underestimated. For the first lockdown period, the inversion increases the total
369 fossil fuel emissions from 2.83 to 3.44 $MtCO_2$ for 2018, from 2.79 to 4.25 $MtCO_2$ for 2019, and
370 from 1.79 to 2.02 $MtCO_2$ for 2020 (the ensemble medians of the posterior estimates from the
371 sensitivity tests are given here). The optimized CO_2 emissions during the first lockdown in 2020
372 show a decrease of around 42% and 53% in fossil fuel CO_2 emissions when compared to the
373 same periods in 2018 and 2019 respectively. For the second lockdown, the changes from prior to
374 posterior total fossil fuel emissions are from 3.13 to 3.33 $MtCO_2$ for 2018, from 3.15 to 3.53
375 $MtCO_2$ for 2019, and from 2.71 to 2.70 $MtCO_2$ for 2020. The total emissions decrease by 19%
376 and 23% in 2020 with respect to 2018 and 2019. In addition, compared to the prior uncertainties,

the inverse emissions reach an uncertainty reduction of about 8~10% for the total emissions. Note that the uncertainties discussed here are relative uncertainties, dependent on the prior emission uncertainties assigned to the Origins inventory.

We examined the full ensemble of inverse emission estimates to identify the most critical assumptions made in the system. First, the sensitivity tests indicate that the inversion with/without assimilating data from the two urban stations (JUS and CDS) produces similar results (NO. 2-4 in Table S3 with respect to the reference). This could be linked to the large model error that was assigned to the urban stations in the inversion system (SI Appendix, Text S7). Regarding the data selection criteria, when assimilating data during the late morning and afternoon (8-17 UTC) (NO. 10 in Table S3, denoted as "day" in Figure 6), we note that the inversion produces lower fossil fuel emission estimates than the reference (which only uses the afternoon data, i.e. 12-17 UTC). This might be due to biases in modeled PBL heights, or to the inadequate depiction of the near-surface vertical mixing, or incorrect diurnal cycles in prior emissions. The inversion solution is also sensitive to the target distance (NO. 12-13 in Table S3, denoted as "tdis20" and "tdis40" in Figure 6) used in the selection of the assimilated CO_2 gradients between pairs of upwind and downwind stations. By filtering out pairs of stations close to each other with a minimum station-to-station distance, we eliminated downwind-upwind gradients that are not representative of a large portion of the urban area. The target distance plays a critical role in determining the number of the assimilated CO_2 data both from the urban-suburb gradients and from the suburb-suburb ones that are representative of urban emissions and the cross-city emissions respectively. This configuration is therefore a primary parameter in our inversion system as the inverse solution is constrained by the selected atmospheric observations. The sensitivity to the temporal error correlations in the prior fossil fuel fluxes is also a critical

parameter, especially during weeks with limited observations filtered out following our criteria (NO. 14-16 in Table S3, denoted as “corr1”, “corr4” and “corr14” in Figure 6). The results show that the values of the relative uncertainty in the prior monthly budgets of fossil fuel emissions (NO. 17-18) and biogenic emissions (NO. 19) have little influence on the inverse solution.

4 Discussions

Our analyses show that the substantial drop in the measured CO_2 concentration enhancements over Paris during the first lockdown in spring 2020 is partly due to a change in meteorological conditions that happened coincidentally with the lockdown measures. Nevertheless, inversion results show that the first lockdown in spring 2020 resulted in a large reduction of emissions, of about 53% and 42% for the Greater Paris region when compared to 2019 and 2018 respectively, while the reductions were estimated to be 37% and 36% based on the Origins inventory. This decrease results from both the large reduction in traffic emissions during the lockdown, and the milder temperature than normal, which has an influence on household emissions. The decrease in emissions during the second lockdown is less pronounced (~20%), due to the continuation of a larger share of economic activity and road traffic. Our inversion results are in line with a bottom-up assessment for CO_2 emissions over Paris communicated by the City of Paris (~50% reduction for March 2020)[29], suggesting that our inversion system is able to quantify monthly city-scale CO_2 variations. The initial assessments given by the AirParif local air quality agency indicate a decrease of about 30% in total CO_2 emissions over the IdF region at the beginning of the first lockdown (March 17th-20th). It also claimed that traffic emissions decreased by 70% during the first lockdown and only about 20% at the beginning of the second lockdown.

Apart from these encouraging results, several challenges and potential improvements inherent to the city-scale atmospheric inversion should also be noted. Our atmospheric inversion retrieves larger fossil fuel CO_2 emissions over the Greater Paris region than the prior estimates, especially for 2019. At this point, we cannot offer a definitive interpretation of this apparent discrepancy between the inventory and the atmospheric inversion estimate. Other socioeconomic data sets and inventory products may provide further insight when they become available in the future. Nevertheless, to provide an alternative evaluation of the capability of the inversion results, we performed an additional sensitivity test by multiplying the prior fossil fuel fluxes by a factor of 2. The results in Figure S10 show that the posterior estimates tend to converge with the reference inversion results, which suggests that our whole-city inverse solution is mostly constrained by atmospheric observations rather than by the prior emissions from the Origins inventory.

Another important aspect of this approach is that the uncertainties in the posterior estimates of CO_2 emissions are caused, to a certain extent, by errors in the spatial and temporal distribution of urban emissions at scales finer than the targeted ones. The configuration of the present inversion systems and the analysis of their outputs primarily target the city-scale monthly budgets rather than emissions at high spatiotemporal resolutions. We limited the spatial resolution of the inversion due to the current configuration of the city observation network with only two stations in the densest part of the urban area (JUS and CDS). Since Bréon et al.[16] and Staufer et al.[11] focusing on the year 2011, the number of CO_2 in situ stations has increased to seven since 2014. The present monitoring network used in this study, in particular the two urban sites, provides enough observations to constrain the whole urban area but additional sites will be needed to estimate the fossil fuel emissions over the Paris inner city (red shaded area in Figure 2). The inversion estimates of the total fossil fuel CO_2 emissions over the city of Paris and the Greater

Paris region (excluding Paris) during the two lockdown periods are shown in Figure S11. Results indicate a larger reduction (in relative) of CO_2 emissions for the city of Paris than that for the Greater Paris region (excluding Paris). It should be noted that there are only two stations within Paris to constrain the inversion, but the extension of the network will allow future inversion studies to separate the inner city from the large suburban area around Paris.

ASSOCIATED CONTENT

Supporting Information

The Supporting Information is available free of charge on the ACS Publications website at DOI: Supporting Information.

Additional details on Origins fossil fuel CO_2 emission inventory, WRF-Chem model configuration, Bayesian inversion setup and supplementary results.

AUTHOR INFORMATION

Corresponding Author

* Jinghui Lian (jinghui.lian@suez.com)

Funding Sources

Thomas Lauvaux is supported by the French research program “Make Our Planet Great Again” (Project CIUDAD).

ACKNOWLEDGMENT

The authors would like to thank Suez Group and the City of Paris for the support of these ongoing analyses. Thanks also to OVSQ, to Marc Jamous at CDS, to the IPSL QUALAIR

platform team and to Cristelle Cailteau-Fischbach (LATMOS/IPSL) for JUS, and to LSCE/RAMCES technical staff for the maintenance of the CO_2 monitoring network.

REFERENCES

1 Le Quéré, C., Jackson, R. B., Jones, M. W., Smith, A. J. P., Abernethy, S., Andrew, R. M., De-Gol, A. J., Willis, D. R., Shan, Y., Canadell, J. G., Friedlingstein, P., Creutzig, F., and Peters, G. P.: Temporary reduction in daily global CO_2 emissions during the COVID-19 forced confinement, Nat. Clim. Change, 10, 647–653, https://doi.org/10.1038/s41558-020-0797-x, 2020.

2 Liu, Z., Ciais, P., Deng, Z., Lei, R., Davis, S. J., Feng, S., Zheng, B., Cui, D., Dou, X., Zhu, B., Guo, R., Ke, P., Sun, T., Lu, C., He, P., Wang, Y., Yue, X., Wang, Y., Lei, Y., Zhou, H., Cai, Z., Wu, Y., Guo, R., Han, T., Xue, J., Boucher, O., Boucher, E., Chevallier, F., Tanaka, K., Wei, Y., Zhong, H., Kang, C., Zhang, N., Chen, B., Xi, F., Liu, M., Breon, F-M., Lu, Y., Zhang, Q., Guan, D., Gong, P., Kammen, D. M., He, K., and Schnellhuber, H. J.: Near-real-time monitoring of global CO_2 emissions reveals the effects of the COVID-19 pandemic, Nat. Commun., 11, 5172, https://doi.org/10.1038/s41467-020-18922-7, 2020.

3 Tollefson, J.: COVID curbed carbon emissions in 2020-but not by much. Nature. https://www.nature.com/articles/d41586-021-00090-3, 2021.

4 Le Quéré, C., Peters, G. P., Friedlingstein, P., Andrew, R. M., Canadell, J. G., Davis, S. J., Jackson, R. B., and Jones, M. W.: Fossil CO_2 emissions in the post-COVID-19 era, Nat. Clim. Change, 11, 197–199, https://doi.org/10.1038/s41558-021-01001-0, 2021.

5 Mueller, K. L., Lauvaux, T., Gurney, K. R., Roest, G., Ghosh, S., Gourdji, S. M., Karion, A., DeCola, P., and Whetstone, J.: An emerging GHG estimation approach can help cities achieve their climate and sustainability goals. Environmental Research Letters, 16(8): 084003, 2021.

6 Turner, A. J., Kim, J., Fitzmaurice, H., Newman, C., Worthington, K., Chan, K., Wooldridge, P. J., Köehler, P., Frankenberg, C., and Cohen, R. C.: Observed impacts of COVID ‐ 19 on urban CO_2 emissions. Geophysical Research Letters, 47(22), e2020GL090037. https://doi.org/10.1029/2020GL090037, 2020.

7 Papale, D., Antoniella, G., Nicolini, G., Gioli, B., Zaldei, A., Vogt, R., Feigenwinter, C., Stagakis, S., Chrysoulakis, N., Järvi, L., Nemitz, E., Helfter, C., Barlow, J., Meier, F., Velasco, E., Christen, A., and Masson, V.: Clear evidence of reduction in urban CO_2 emissions as a result of COVID-19 lockdown across Europe. Integrated Carbon Observation System (ICOS), https://energypress.gr/sites/default/files/media/meleti.pdf, 2020.

8 Venturi, S., Randazzo, A., Tassi, F., Gioli, B., Buccianti, A., Gualtieri, G., Capecchiacci, F., Cabassi, J., Brilli, L., Carotenuto,F., Santi, R., Vagnoli, C., Zaldei, A., and Vaselli, O.: Unveiling the changes in urban atmospheric CO_2 in the time of COVID-19 pandemic: A case study of Florence (Italy). Science of The Total Environment, 148877, https://doi.org/10.1016/j.scitotenv.2021.148877, 2021.

9 Liu, D., Sun, W., Zeng, N., Han, P., Yao, B., Liu, Z., Wang, P., Zheng, K., Mei, H., and Cai, Q.: Observed decreases in on-road CO_2 concentrations in Beijing during COVID-19 restrictions, Atmos. Chem. Phys., 21, 4599–4614, https://doi.org/10.5194/acp-21-4599-2021, 2021.

10 You, Y., Byrne, B., Colebatch, O., Mittermeier, R. L., Vogel, F., and Strong, K.: Quantifying the impact of the COVID-19 pandemic restrictions on CO, CO_2, and CH_4 in downtown Toronto using open-path fourier transform spectroscopy. Atmosphere, 12(7), 848, https://doi.org/10.3390/atmos12070848, 2021.

11 Staufer, J., Broquet, G., Bréon, F.-M., Puygrenier, V., Chevallier, F., Xueref-Rémy, I., Dieudonné, E., Lopez, M., Schmidt, M., Ramonet, M., Perrussel, O., Lac, C., Wu, L., and Ciais, P.: The first 1-year-long estimate of the Paris region fossil fuel CO_2 emissions based on atmospheric inversion, Atmos. Chem. Phys., 16, 14703–14726, https://doi.org/10.5194/acp-16-14703-2016, 2016.

12 Sargent, M., Barrera, Y., Nehrkorn, T., Hutyra, L. R., Gately, C. K., Jones, T., McKain, K., Sweeney, C., Hegarty, J., Hardiman, B., Wang, J. A., and Wofsy, S. C.: Anthropogenic and biogenic CO_2 fluxes in the Boston urban region. Proceedings of the National Academy of Sciences, 115(29), 7491-7496, 2018.

13 Lauvaux, T., Gurney, K. R., Miles, N. L., Davis, K. J., Richardson, S. J., Deng, A., Nathan, B. J., Oda, T., Wang, J. A., Hutyra, L., and Turnbull, J.: Policy-Relevant Assessment of Urban CO_2 Emissions, Environ. Sci. Technol., 54, 10237–10245, https://doi.org/10.1021/acs.est.0c00343, 2020.

14 Lauvaux, T., Miles, N. L., Richards, S. J., Deng, A., Stauffer, D. R., Davis, K. J., Jacobson, G., Rella, C., Calonder, G.-P., and DeCola, P. L.: Urban emissions of CO_2 from Davos, Switzerland: The first real-time monitoring system using an atmospheric inversion technique. Journal of Applied Meteorology and Climatology, 52(12), 2654–2668, https://doi.org/10.1175/JAMC-D-13-038.1, 2013.

15 Yadav, V., Ghosh, S., Mueller, K., Karion, A., Roest, G., Gourdji, S. M., Lopez-Coto, I., Gurney, K. R., Parazoo, N., Verhulst, K. R., Kim, J., Prinzivalli, S., Fain, C., Nehrkorn, T., Mountain, M., Keeling, R. F., Weiss, R. F., Duren, R., Miller, C. E., and Whetstone, J.: The impact of COVID‐19 on CO_2 emissions in the Los Angeles and Washington DC/Baltimore metropolitan areas. Geophysical Research Letters, 48(11), https://doi.org/10.1029/2021GL092744, 2021.

16 Bréon, F. M., Broquet, G., Puygrenier, V., Chevallier, F., Xueref-Remy, I., Ramonet, M., Dieudonné, E., Lopez, M., Schmidt, M., Perrussel, O., and Ciais, P.: An attempt at estimating Paris area CO_2 emissions from atmospheric concentration measurements, Atmos. Chem. Phys., 15, 1707–1724, https://doi.org/10.5194/acp-15-1707-2015, 2015.

17 Lian, J., Wu, L., Bréon, F. M., Broquet, G., Vautard, R., Zaccheo, T. S., Dobler, J., and Ciais, P.: Evaluation of the WRF-UCM mesoscale model and ECMWF global operational forecasts over the Paris region in the prospect of tracer atmospheric transport modeling. Elem. Sci. Anth., 6, 64, https://doi.org/10.1525/elementa.319, 2018.

18 Lian, J., Bréon, F. M., Broquet, G., Zaccheo, T. S., Dobler, J., Ramonet, M., Staufer, J., Santaren, D., Xueref-Remy, I., and Ciais, P.: Analysis of temporal and spatial variability of atmospheric CO_2 concentration within Paris from the GreenLITE™ laser imaging experiment. Atmos. Chem. Phys., 19, 13809–13825, https://doi.org/10.5194/acp-19-13809-2019, 2019.

19 Lian, J., Bréon, F.-M., Broquet, G., Lauvaux, T., Zheng, B., Ramonet, M., Xueref-Remy, I., Kotthaus, S., Haeffelin, M., and Ciais, P.: Sensitivity to the sources of uncertainties in the

549 modeling of atmospheric CO_2 concentration within and in the vicinity of Paris, Atmos.
550 Chem. Phys., 21, 10707–10726, https://doi.org/10.5194/acp-21-10707-2021, 2021.

551 20 Wang, Y., Deng, Z., Ciais, P., Liu, Z., Davis, S. J., Gentine, P., Lauvaux, T., and Ge, Q.:
552 Transportation CO_2 emissions stayed high despite recurrent COVID outbreaks. arXiv
553 preprint arXiv:2101.06450, https://arxiv.org/abs/2101.06450, 2021.

554 21 Bulletin Climatique Météo-France:
555 https://donneespubliques.meteofrance.fr/?fond=produit&id_produit=129&id_rubrique=29
556 (last access: 5 July 2021), 2019, 2020.

557 22 Ciais, P., Bréon, F. M., Dellaert, S., Wang, Y., Tanaka, K., Gurriaran, L., Françoise, Y.,
558 Davis, S.J., Hong, C., Penuelas, J., Janssens, I., Obersteiner, M., Deng, Z., and Liu, Z.:
559 Impact of lockdowns and winter temperatures on natural gas consumption in Europe. Earth's
560 Future, https://doi.org/10.1029/2021EF002250, 2021.

561 23 Tans, P., Zhao, C., and Kitzis, D.: The WMO Mole Fraction Scales for CO2 and other
562 greenhouse gases, and uncertainty of the atmospheric measurements, Report of the 15th
563 WMO/IAEA Meeting of Experts on Carbon Dioxide, Other Greenhouse Gases, and Related
564 Measurement Techniques, 7-10 September 2009, GAW Report No. 194, WMO TD No.
565 1553, 152–159, 2011.

566 24 Wu, L., Broquet, G., Ciais, P., Bellassen, V., Vogel, F., Chevallier, F., Xueref-Remy, I., and
567 Wang, Y.: What would dense atmospheric observation networks bring to the quantification
568 of city CO_2 emissions?, Atmos. Chem. Phys., 16, 7743–7771, https://doi.org/10.5194/acp-
569 16-7743-2016, 2016.

25 Oda, T. and Maksyutov, S.: A very high-resolution (1 km×1 km) global fossil fuel CO_2 emission inventory derived using a point source database and satellite observations of nighttime lights, Atmos. Chem. Phys., 11, 543–556, https://doi.org/10.5194/acp-11-543-2011, 2011.

26 Nassar, R., Napier-Linton, L., Gurney, K. R., Andres, R. J., Oda, T., Vogel, F. R., and Deng, F.: Improving the temporal and spatial distribution of CO_2 emissions from global fossil fuel emission data sets, J. Geophys. Res., 118, 917–933, https://doi:10.1029/2012JD018196, 2013.

27 Mahadevan, P., Wofsy, S. C., Matross, D. M., Xiao, X., Dunn, A. L., Lin, J. C., Gerbig, C., Munger, J. W., Chow, V. Y., and Gottlieb, E. W.: A satellite-based biosphere parameterization for net ecosystem CO_2 exchange: Vegetation Photosynthesis and Respiration Model (VPRM). Global Biogeochem. Cy., 22, GB2005, https://doi.org/10.1029/2006GB002735, 2008.

28 Ahmadov, R., Gerbig, C., Kretschmer, R., Koerner, S., Neininger, B., Dolman, A. J., and Sarrat, C.: Mesoscale covariance of transport and CO_2 fluxes: Evidence from observations and simulations using the WRF-VPRM coupled atmosphere-biosphere model. J. Geophys. Res.-Atmos., 112, D22107, https://doi.org/10.1029/2007JD008552, 2007.

29 Ciais, P., Ramonet, M., Lauvaux, T., Bréon, F. M., Lian, J., Laurent, O., Combaz, D., Broquet, G., Legendre, V., Delmotte, M., Xueref-Rémy, I., Jamous, M., Cailteau-Fischbach, C., Françoise, Y. : Suivi atmosphérique des émissions de CO_2 de la région parisienne. La Météorologie. n° 114, 2021.